Density Functional Study of the Photodissociation of $Mn_2(CO)_{10}$

Angela Rosa,[†] Giampaolo Ricciardi,[†] Evert Jan Baerends,*[,‡] and Derk J. Stufkens[§]

Dipartimento di Chimica, Università della Basilicata, Via N. Sauro, 85, 85100 Potenza, Italy, Afdeling Theoretische Chemie, Vrije Universiteit, De Boelelaan 1083, 1081 HV Amsterdam, The Netherlands, and Anorganisch Chemisch Laboratorium, Nieuwe Achtergracht 166, Universiteit van Amsterdam, 1018 WV Amsterdam, The Netherlands

Received April 26, 1995[⊗]

Potential energy curves (PECs) have been calculated for a number of excited states of $Mn_2(CO)_{10}$, along the Mn−Mn bond dissociation coordinate and along $Mn-CO_{ax}$ and $Mn-CO_{eq}$ coordinates, in order to understand why irradiation into the $\sigma \rightarrow \sigma^*$ band does not only lead to Mn−Mn bond breaking but also to Mn−CO dissociation. Mn−Mn bond homolysis can straightforwardly occur along the dissociative $\sigma \rightarrow \sigma^*$ $^3B_2$ PEC. The $\sigma \rightarrow \sigma^*$ excited state is not itself Mn−CO dissociative. CO dissociation occurs since PECs that correspond at equilibrium geometry to $d_{\pi^*} \rightarrow \sigma^*$ $^{1,3}E_1$ excited states (nearly degenerate with the $\sigma \rightarrow \sigma^*$ excited state) are $Mn-CO_{ax}$ dissociative (both $^1E_1$ and $^3E_1$, $^{1,3}E$ in C_{4v}) or $Mn-CO_{eq}$ dissociative (only just, and only the b^3A' component (in C_s) of $^3E_1$). The Mn−CO dissociative character has been traced to the precipitous lowering of the initially high-lying Mn−CO σ-antibonding ($3d(e_g)$-like) orbitals upon Mn−CO bond lengthening, making them considerably lower than σ^* in $Mn_2(CO)_9$. Excitations to these orbitals (the ligand-field (LF) excitations) are at high energy in $Mn_2(CO)_{10}$, much higher than the $\sigma \rightarrow \sigma^*$ and $d_{\pi^*} \rightarrow \sigma^*$ excitations. However, the energy of these LF excited states very rapidly goes down upon Mn−CO bond lengthening, they cross the $\sigma \rightarrow \sigma^*$ and $d_{\pi^*} \rightarrow \sigma^*$ excited states, and the energy lowering of the LF excitation energy in $Mn_2(CO)_9$ with respect to the lowest excitation energies in $Mn_2(CO)_{10}$, to $^{1,3}B_2$ $\sigma \rightarrow \sigma^*$ and $^{1,3}E_1$ $d_{\pi^*} \rightarrow \sigma^*$, provides the energy for the Mn−CO bond breaking.

Introduction

The photochemistry of $Mn_2(CO)_{10}$ in solution has been much studied and is generally taken as a prototype for photoreactions of organometallic compounds containing metal−metal bonds.[1−4] Recently, however, it has been established[5−13] in the condensed-phase photolysis of $Mn_2(CO)_{10}$ that apart from the metal−metal bond cleavage to produce $Mn(CO)_5$ radicals (eq 1), a second

$$Mn_2(CO)_{10} \xrightarrow{h\nu} 2Mn(CO)_5 \qquad (1)$$

primary photochemical reaction pathway exists upon irradiation into the lowest band, namely, dissociative loss of CO to give $Mn_2(CO)_9$ without metal−metal bond cleavage (eq 2). The relative quantum yield for these two channels in fact depends

$$Mn_2(CO)_{10} \xrightarrow{h\nu} Mn_2(CO)_9 + CO \qquad (2)$$

on the excitation wavelength. Generally it was found that low-energy excitation favors metal−metal bond homolysis, while higher energy excitation leads mostly to the generation of $Mn_2(CO)_9$. Kobayashi *et al.*[14] have measured the quantum yields of processes 1 and 2, Y_1 and Y_2, at different excitation wavelengths. They obtained a ratio $R = Y_1/Y_2$ of 0.19, 0.43, and 1.1 at $\lambda_{ex} = 266$, 337, and 355 nm, respectively.

Gas-phase photodissociation studies[15] of $Mn_2(CO)_{10}$ are consistent with the photochemistry of the molecule in solution. Excitation at 350 nm of $Mn_2(CO)_{10}$ in the gas-phase produces Mn−Mn bond homolysis and CO loss, while excitation at 248 and 193 nm only leads to CO loss. In spite of the intense experimental work on the photochemistry of $Mn_2(CO)_{10}$ developed during the past decade, thanks to the availability of very sophisticated identification techniques, the mechanism of the primary photochemical processes is far from being understood. Whether Mn−Mn and Mn−CO cleavage originate from the same or from different excited states and why the relative quantum yields of the photoproducts depend on the excitation wavelength are still crucial questions concerning the photochemistry of $Mn_2(CO)_{10}$ that are basically unanswered. With the aim of locating the possible photoactive excited states of $Mn_2(CO)_{10}$, we have recently investigated[16] the nature of the excited states involved in the electronic spectrum of this compound and their corresponding excitation energies. A significant point to arise from our calculations is that only two transitions, i.e., $d_{\pi^*} \rightarrow \sigma^*$ ($8e_3 \rightarrow 10b_2$) and $\sigma \rightarrow \sigma^*$ ($10a_1 \rightarrow 10b_2$) are responsible for the low-energy excitations (bands I

[†] Università della Basilicata.
[‡] Vrije Universiteit.
[§] Universiteit van Amsterdam.
[⊗] Abstract published in *Advance ACS Abstracts,* April 1, 1996.

(1) (a) Geoffroy, G. L.; Wrighton, M. S. *Organometallic Photochemistry*; Academic: New York, 1979. (b) Geoffroy, G. L. *J. Chem. Educ.* **1983**, *60*, 861.
(2) Wegman, R. W.; Olsen, R. J.; Gard, D. R; Faulkner, L. R.; Brown, T. L. *J. Am. Chem. Soc.* **1981**, *103*, 6089.
(3) Wrighton, M. S.; Ginley, D. S. *J. Am. Chem. Soc.* **1975**, *97*, 2065.
(4) Stufkens, D. J. *Coord. Chem. Rev.* **1990**, *104*, 39.
(5) Yasufuku, K.; Kobayashi, T.; Iwai, J.; Yesaka, H.; Noda, H.; Ohtani, H. *Coord. Chem. Rev.* **1985**, *64*, 1.
(6) Rothberg, L. J.; Cooper, N. J.; Peters, K. S.; Vaida, V. *J. Am. Chem. Soc*, **1984**, *104*, 3536.
(7) Church, S. P.; Herman, H.; Grevels, F.-W.; Schaffner, K. *J. Chem. Soc., Chem. Commun.* **1984**, 785, and references cited therein.
(8) Hepp, A. F.; Wrighton, M. S. *J. Am. Chem. Soc.* **1983**, *105*, 5934.
(9) Leopold, D. G.; Vaida, V. *J. Am. Chem. Soc.* **1984**, *106*, 3720.
(10) (a) Walker, H. W.; Herrick, R. S.; Olsen, R. J; Brown, T. L. *Inorg. Chem.* **1984**, *23*, 3748. (b) Herrick, R. S.; Brown, T. L. *Inorg. Chem.* **1984**, *23*, 4550.
(11) Yesaka, H.; Kobayashi, T.; Yasufuku, K.; Nagakura, S. *J. Am. Chem. Soc.* **1983,** *105*, 6249.
(12) Zhang, J. Z.; Harris, C. B.; *J. Chem. Phys.* **1991**, *95*, 4024.
(13) Joly, A. G.; Nelson, K. A. *Chem. Phys.* **1991**, *152*, 69.
(14) Kobayashi, T.; Ohtani, H.; Noda, H.; Teratani, S.; Yamazaki, H.; Yasufuku, K. *Organometallics* **1986**, *5*, 110.
(15) Prinslow, D. A.; Vaida, V. *J. Am. Chem. Soc.* **1987**, *109*, 5097.
(16) Rosa, A.; Ricciardi, G.; Baerends, E. J.; Stufkens, D. J. *Inorg. Chem.* **1995**, *34*, 3425.

S0020-1669(95)00518-0 CCC: $12.00

and II) at 337−375 nm. [We stick to a notation where σ, π, and δ labels refer to the Mn−Mn axis and σ, σ^*, π, π^*, δ, and δ^* indicate the Mn−Mn bonding respectively, antibonding character of the MO.] Possibly Mn−CO dissociative ligand field (LF) states are not close but occur at much higher energies. Excitation at low energy, in the experimental range 337−355 nm, will then bring the molecule either into the $\sigma \rightarrow \sigma^*$ $^1B_2$ or into the $d_{\pi^*} \rightarrow \sigma^*$ $^1E_1$ spin allowed excited state. This implies that the states arising from $d_{\pi^*} \rightarrow \sigma^*$ and $\sigma \rightarrow \sigma^*$ dominate the photochemistry of $Mn_2(CO)_{10}$ upon excitation in the range 337−355 nm.

There can be little doubt that the respectively Mn−Mn bonding and antibonding nature of the σ and σ^* with respect to metal−metal cleavage makes the state B_2 corresponding to the $\sigma \rightarrow \sigma^*$ excitation photoactive with respect to Mn−Mn cleavage. However, we have found a remarkable lack of metal−CO antibonding character in the σ^* orbital, and it seems unlikely that either the $\sigma \rightarrow \sigma^*$ B_2 state or the $d_{\pi^*} \rightarrow \sigma^*$ E_1 state would lead to CO loss. However, even if these states would not be photoactive by themselves for the dissociation of a carbonyl ligand, photodissociation of a carbonyl ligand at low energy might still occur upon excitation in these states if crossing occurs to the potential energy surfaces of excited states which *are* dissociative with respect to a metal−carbonyl bond. In our previous study we have identified LF type excitations to states that are probably $Mn-CO_{ax}$ dissociative (basically $d \rightarrow \sigma'$) and to states that are probably $Mn-CO_{eq}$ dissociative ($d \rightarrow d_\delta(e_g)$). We recall that we have denoted in our previous paper[16] as σ' and σ'^* the $11a_1$ and $11b_2$ MOs, with considerable d_{z^2} character, that are quite strongly antibonding with respect to the axial carbonyl ligands. The $d_\delta(e_g)$ is the high-lying $9e_2$ ($d_{x^2-y^2}$) which is strongly antibonding with the 5σ's of the equatorial COs.

Since these presumably Mn−CO dissociative $d \rightarrow d$ excitations occur at much higher energy than the $\sigma \rightarrow \sigma^*$ and $d_{\pi^*} \rightarrow \sigma^*$ excitations, explicit calculations of potential energy surfaces (PESs) or the more readily visualized potential energy curves (PECs) are required to verify the crossing suggested above as possible explanation for the Mn−CO dissociation. The PEC curves provide the most important features of the energy profile of the primary photodissociative pathways, as proved for a number of organometallic systems.[17−24] We have calculated, using a density functional approach, the ground- and excited-state potential energy curves corresponding to the homolysis of the Mn−Mn bond and to the dissociation of an axial as well as an equatorial carbonyl ligand.

Method and Computational Details

The calculations reported in this paper are based on the Amsterdam density functional (DF) program package[25,26] characterized by the use of a density fitting procedure to obtain accurate Coulomb and exchange potentials in each self-consistent field (SCF) cycle, by accurate and efficient numerical integration of the effective one-electron Hamiltonian matrix elements and by the possibility to freeze core orbitals.

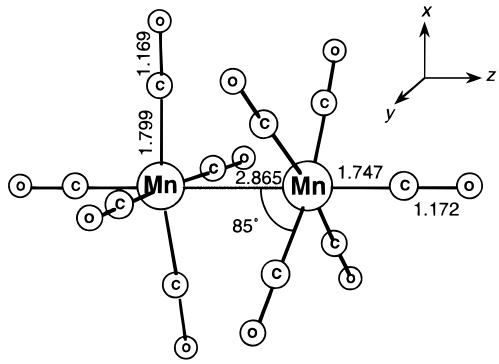

Figure 1. Optimized structure of $Mn_2(CO)_{10}$ in D_{4d} symmetry[16] (bond distances in angstroms).

In order to improve the reliability of the computed potential energy curves, the integration accuracy and the fit set have been increased with respect to our previous calculations[16] of the ground and excited states of $Mn_2(CO)_{10}$.

The molecular orbitals were expanded in an uncontracted double-ζ STO basis set for all atoms with the exception of the 3d Mn orbitals for which we used a triple-ζ STO basis set. As polarization functions one 4p STO was used for Mn atom. The cores (Mn, 1s−2p; C, O, 1s) have been kept frozen.

Three theoretical DF models have been adopted in the calculation of the energies of the reactants, of the products as well as of the dissociating system along the reaction paths, i.e, (i) the local spin density approximation, LSDA, characterized by the electron gas exchange (Xα with $\alpha = {}^2/_3$)[27] together with the Vosko−Wilk−Nusair[28] parametrization for correlation; (ii) the LSDA plus Becke's[29] nonlocal corrections to the exchange energy; (iii) the LSDA plus Becke's nonlocal corrections to the exchange energy and Perdew's[30] nonlocal corrections to the correlation energy. However, we will report here only the potential energy curves calculated including both Becke's and Perdew's nonlocal corrections. This model represents to date one of the most efficient and accurate methods for the evaluation of bond energies within a DF framework, as shown by calculations on metal carbonyls,[31] binuclear metal complexes[32] including $Mn_2(CO)_{10}$ (see next sections), alkyl and hydride complexes,[33] and complexes containing metal−ligand bonds for a number of different ligands.[34]

The calculations for $Mn_2(CO)_{10}$ were performed for the optimized[16] geometry in D_{4d} experimental symmetry (Figure 1). Potential energy curves were computed for the reaction paths corresponding to the Mn−Mn cleavage (Scheme 1), the loss of an axial (Scheme 2), and an equatorial (Scheme 3) carbonyl ligand, with the following assumptions:

(i) D_{4d} symmetry is retained along the reaction path corresponding to the homolysis of the metal−metal bond. Support for this assumption comes from the fact that $Mn(CO)_5$ has C_{4v} symmetry in its ground state.[24,35,36] Bond lengths (except for the bond which dissociates) and

(17) Daniel, C.; Bénard, M.; Dedieu, A.; Wiest, R.; Veillard, A. *J. Phys. Chem.* **1984**, *88*, 4805.
(18) Daniel, C.; Hyla-Kryspin, I.; Demuynck, J.; Veillard, A. *Nouv. J. Chim.* **1985**, *9*, 581.
(19) Veillard, A.; Daniel, C.; Strich, A. *Pure Appl. Chem.*, **1988**, *60* (2), 215.
(20) Veillard, A.; Strich, A. *J. Am. Chem. Soc.* **1988**, *110*, 3793.
(21) Daniel, C. *Proceedings of the 8th International Symposium on the Photochemistry and Photophysics of Coordination Compounds*; Coordination Chemistry Reviews, Elsevier Science Publishers B. V.: Amsterdam, 1990; Vol. 97, p 141.
(22) Daniel, C. *J. Phys. Chem.* **1991**, *95*, 2394.
(23) Rohmer, M. M.; Veillard, A. *New J. Chem.* **1991**, *15*, 795.
(24) Daniel, C. *J. Am. Chem. Soc.* **1992**, *114*, 1625.
(25) (a) Baerends, E. J.; Ellis, D. E.; Ros, P. *Chem. Phys.* **1973**, *2*, 42. (b) Baerends, E. J.; Ros, P. *Int. J. Quantum Chem.***1978**, *S12*, 169.
(26) (a) Boerrigter, P. M.; te Velde, G.; Baerends, E. J.; *Int. J. Quantum Chem*, **1988**, *33*, 87. (b) te Velde, G.; Baerends, E. J. *J. Comput. Phys.* **1992**, *99*, 84.
(27) Parr, R. G.; Yang,W. *Density-Functional Theory of Atoms and Molecules*; Oxford University Press: New York, 1989.
(28) Vosko, S. H.; Wilk, L.; Nusair, M. *Can. J. Phys.* **1980**, *58*, 1200.
(29) (a) Becke, A. D. *J. Chem. Phys.* **1986**, *84*, 4524. (b) Becke, A. D. *Phys. Rev.* **1988**, *A38*, 3098.
(30) (a) Perdew, J. P. *Phys. Rev.* **1986**, *B33*, 8822. (b) Perdew, J. P.*Phys. Rev.* **1986**, *B34*, 7406.
(31) Ziegler, T.; Tschinke, V.; Ursenbach, C. *J. Am. Chem. Soc.* **1987**, *109*, 4825.
(32) Ziegler, T.; Tschinke, V.; Becke, A. *Polyhedron* **1987**, *6*, 685.
(33) (a) Ziegler, T.; Tschinke, V.; Becke, A. *J. Am. Chem. Soc.* **1987**, *109*, 1351. (b) Ziegler, T.; Cheng, W.; Baerends, E. J.; Ravenek, W. *Inorg. Chem.* **1988,** *27*, 3458. (c) Ziegler, T.; Tschinke, V.; Baerends, E. J.; Snijders, J. G.; Ravenek, W. *J. Phys. Chem.* **1989**, *93*, 3050. (d) Ziegler, T.; Baerends, E. J.; Snijders, J. G. *J. Chem. Phys.* **1981**, *74*, 5737.
(34) Ziegler, T.; Tschinke, V.; Versluis, L.; Baerends, E. J.; Ravenek, W. *Polyhedron* **1988**, *7*, 1625.

Scheme 1

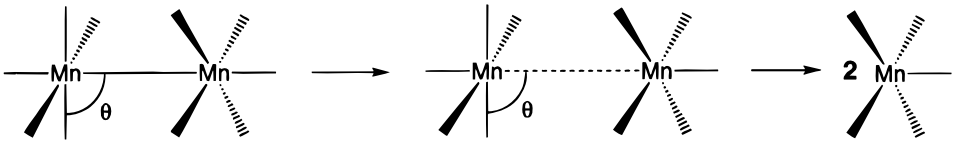

Scheme 2

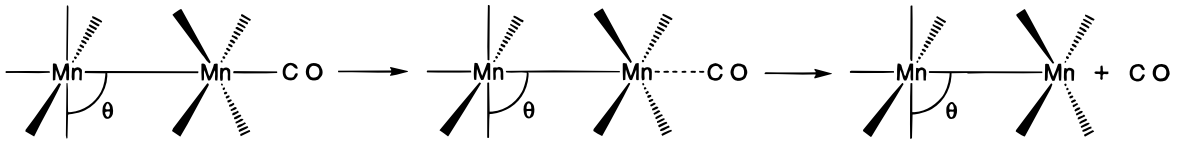

Scheme 3

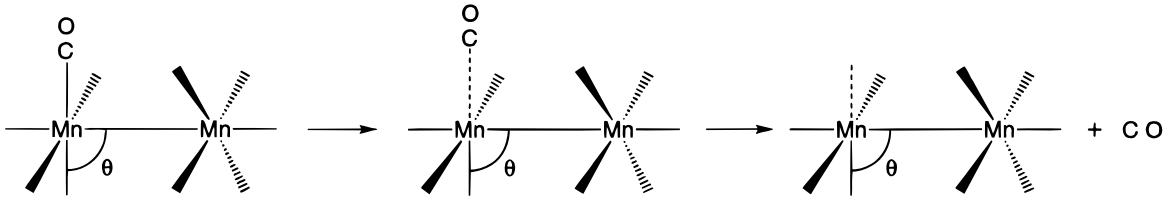

the angle $\angle C_{eq}MnMn$, θ, were optimized for each point along the reaction path. Geometry optimizations have always been performed at the LSDA level of theory using gradient techniques.[37]

(ii) C_{4v} and C_s symmetries respectively are retained along the reaction paths corresponding to the loss of an axial and an equatorial CO. By this hypothesis we assume that the primary product, $Mn_2(CO)_9$, is formed in a purely metal−metal bonded structure of C_{4v} or C_s symmetry with an axial or an equatorial vacancy. Support for this assumption comes from the fact that, as has been recently demonstrated,[12,38,39] the formation of a linear semibridged structure, $Mn_2(CO)_8(\mu\text{-}\eta^1{:}\eta^2\text{-CO})$ occurs only via secondary photolysis of a solvento species, $Mn_2(CO)_9$(solv), which is clearly the initial product following CO loss.

As for the dissociation of an axial CO, all geometrical parameters, except for the dissociating bond, were optimized for all the points on the potential energy curve.

As for the dissociation of an equatorial CO, in order to keep the calculations tractable, the bond parameters, except for the bond which dissociates, were kept constant along the reaction pathway. This assumption is justified by the following arguments: (i) the optimized structure of $Mn_2(CO)_9$ of C_s symmetry derived from $Mn_2(CO)_{10}$ with an equatorial vacancy does not show significant differences compared to the not optimized one; (ii) during the reaction path corresponding to the axial CO loss the geometrical parameters also remain almost unchanged.

Excitation energies and singlet/triplet splittings have been computed according to the method by Ziegler *et al.*[40] It is well-known that excited states have a different status within DFT than the ground state. Attempts to put the calculation of excited state energies on a similar basis as ground state energies[41] have not yet led to practical schemes due to the theoretically defined functionals being unknown. Just using existing approximate functionals in this scheme[42] leads to rather poor agreement with experiment. The method of ref 40 has been shown to lead to quite good excitation energies and multiplet splittings for many molecules, including transition-metal complexes,[40,43−45] and for atoms.[46−48] It should be pointed out that, for the lowest state of a given symmetry, the Kohn−Sham (KS) single-determinantal treatment that is the basis of the current method,[40] has the same status as for ground states.[49] This implies that also in cases where the exact wave function can only be described correctly by invoking configuration interaction, as is the case at and close to avoided crossings, the DFT energies from the single-determinantal Kohn−Sham calculations are still reliable (although of course the KS determinant is not a good approximation to the wave function then). There is now considerable evidence that the present gradient-corrected functionals, like the Becke−Perdew one we are using, yield quite accurate transition-state barriers on the ground state potential energy surface during a reaction.[50] This would then be expected to hold true for an avoided crossing type barrier on the first excited state surface of a given symmetry as well. Our conclusions will all refer to these lowest excited state surfaces. We will also calculate higher excited states with the current method, as has been successfully done before at equilibrium geometries, but we will keep in mind the possibly larger errors for those excited state energies and will avoid overinterpreting them.

Metal−Metal Photodissociation

Before we comment on the essential features of the curves of the excited states connecting the reactant to the products along the reaction path shown in Scheme 1, it is useful to check whether the structures of the reactant and the products and their relative stabilities are correctly reproduced by our calculations, since this will ensure that the potential energy curves have the right slope.

As concerns the primary photoproduct following the homolysis of the Mn−Mn bond, $Mn(CO)_5$ radical, experiments by Church *et al.*[35] have demonstrated that this species has square-

(35) Church, S. P.; Poliakoff, M.; Timney, J. A.; Turner, J. J. *J. Am. Chem. Soc.* **1981**, *103*, 7515.
(36) MacNeil, J. H.; Chiverton, A. C.; Fortier, S.; Baird, M. C.; Hynes, R. C.; Williams, A. J.; Preston, K. F.; Ziegler, T. *J. Am. Chem. Soc.* **1991**, *113*, 9834.
(37) Versluis, L.; Ziegler, T. *J. Chem. Phys.* **1988**, *88*, 322.
(38) Zhang, S.; Zhang, H.-T.; Brown, T. L. *Organometallics* **1992**, *12*, 3929.
(39) Waldman, A.; Ruhman, S.; Shaik, S.; Sastry, G. N. *Chem. Phys. Lett.* **1994**, *230*, 110.
(40) Ziegler, T.; Rauk, A.; Baerends, E. J. *Theoret. Chim. Acta* **1977**, *43*, 261.
(41) (a) Gross, E. K. U.; Oliveira, L. N.; Kohn, W. *Phys. Rev.* **1988**, *A37*, 2805. (b) Gross, E. K. U.; Oliveira, L. N.; Kohn, W. *Phys. Rev.* **1988**, *A37*, 2809. (c) Gross, E. K. U.; Oliveira, L. N.; Kohn, W. *Phys. Rev.* **1988**, *A37*, 2821.
(42) Nagy, A.; Andrejkovics, I. *J. Phys.* **1994**, *B27*, 233.
(43) (a) Ziegler, T.; Nagle, J. K.; Snijders, J. G.; Baerends, E. J. *J. Am. Chem. Soc.* **1989**, *111*, 5631. (b) Ziegler, T. *Inorg. Chem.* **1993**, *32*, 2029.
(44) Rosa, A.; Baerends, E. J. *Inorg. Chem.* **1994**, *33*, 584.
(45) Daul, C.; Baerends, E. J.; Vernooijs, P. *Inorg. Chem.* **1994**, *33*, 3543.
(46) von Barth, U. *Phys. Rev.* **1979**, *A20*, 1693.
(47) Lannoo, M.; Baraff, G. A.; Schlüter, M. *Phys. Rev.* **1981**, *B24*, 943.
(48) Wood, J. H. *J. Phys. B*: *At. Mol. Phys.* **1980**, *13*, 1.
(49) Gunnarsson, O.; Lundqvist, B. I. *Phys. Rev.* **1976**, *B13*, 4274.
(50) (a) Deng, L.; Ziegler, T. *Int. J. Quantum Chem.* **1994**, *52*, 731. (b) Deng, L.; Branchadell, V.; Ziegler, T. *J. Am. Chem. Soc.* **1994**, *116*, 10645. (c) Fan, L.; Ziegler, T. *J. Am. Chem. Soc.* **1992**, *114*, 10890.

Table 1. Comparison of the Calculated Metal−Metal Bond Energy, D(Mn−Mn), and First Ligand Dissociation Energies in $Mn_2(CO)_{10}$ with Experiments (Bond Energies, kJ mol^{-1})

method	E^{LSDA} [a]	$E^{LSDA}+E_x^{NL}$ [b]	$E^{LSDA}+E_x^{NL}+E_c^{NL}$ [c]	expt
D(Mn−Mn)[d]	258	28	135	104 ± 3;[e] 79 ± 14;[f] 88 ± 13;[g] 94;[h] ≥154;[i] 171;[l] 159 ± 21;[m] ≥176[n]
$\Delta H_{ax}{}^{o}$	305	126	200	
$\Delta H_{eq}{}^{o}$	292	73	177	159[q]
$\Delta H_{sb}{}^{p}$	261	76	165	

[a] Bonding energy calculated by LSDA method. [b] Bonding energy calculated combining nonlocal exchange correction by Becke with LSDA. [c] Bonding energy calculated combining nonlocal corrections of both Becke and Perdew with LSDA. [d] The calculated bonding energy D(Mn−Mn) = [$2\Delta E_{MnCO_5} - \Delta E_{Mn_2CO_{10}}$] is with respect to the fragments in their ground state optimized geometries. [e] Electron impact mass spectrometry from ref 56. [f] Electron impact mass spectrometry from ref 57. [g] Equilibrium studies using electron impact mass spectrometry from ref 57. [h] Thermochemical estimate from ref 58. [i] Kinetic studies in solution from refs 59 and 60. [l] Electron impact mass spectrometry/photoelectron spectroscopy from ref 61. [m] Photoacoustic calorimetry determination from ref 62. [n] Laser pyrolysis from ref 63. [o] The axial and equatorial CO dissociation energies, ΔH_{ax} and ΔH_{eq}, corresponding to the process $Mn_2(CO)_{10} \rightarrow Mn_2(CO)_9 + CO - \Delta H$, is with respect to CO and a $Mn_2(CO)_9$ fragment in a purely metal−metal bonded structure with an axial or equatorial vacancy, optimized within C_{4v} or C_s symmetry constraint (see Figure 3a,b). [p] The first ligand dissociation energy, $\Delta H°_{sb}$, corresponding to the process $Mn_2(CO)_{10} \rightarrow Mn_2(CO)_9 + CO - \Delta H$ is with respect to CO and a $Mn_2(CO)_9$ fragment in a semibridged structure optimized within C_s symmetry constraint (see Figure 3d). [q] References 63 and 65.

pyramidal, C_{4v} structure with an apical-basal Mn−CO bond angle of 96 ± 3°, and recent calculations[26,51] also give the C_{4v} structure as the most stable one. The geometry of $Mn_2(CO)_{10}$ has been investigated by electron diffraction in the gas phase[52] and by X-ray diffraction at room temperature[53] and at 74 K.[54] All of these experiments lead to nearly the same geometry, which is consistent with a D_{4d} symmetry. Density functional calculations by Folga and Ziegler[51] give the eclipsed structure (D_{4h}) higher in energy by 142.4 kJ mol^{-1} than the staggered one. Since the $Mn(CO)_5$ (C_{4v}) and $Mn_2(CO)_{10}$ (D_{4d}) optimized structures that we have recently calculated[16] show reasonable agreement between theoretical and experimental geometries, we stick here to those geometries.

From the values of Table 1, where we report the metal−metal bond energy D(Mn−Mn) calculated using different theoretical DF models, the process $Mn_2(CO)_{10} \rightarrow 2Mn(CO)_5$ is calculated to be endothermic. One will notice that the LSDA overestimates considerably the metal−metal bond energy; the addition of Becke's nonlocal exchange correction yields a bond energy which is much too low. Adding however the nonlocal correlation correction yields a metal−metal bond energy which is in the range of the most recent experimental values obtained for D(Mn−Mn).[55−63] Due to limitations in the present calculations, in particular with respect to the basis set, the theoretical value for D(Mn−Mn) is not the definitive density functional result, but it should be fairly close. We will present a comprehensive treatment of the effect of computational approximations to D(Mn−Mn) and other quantities elesewhere.

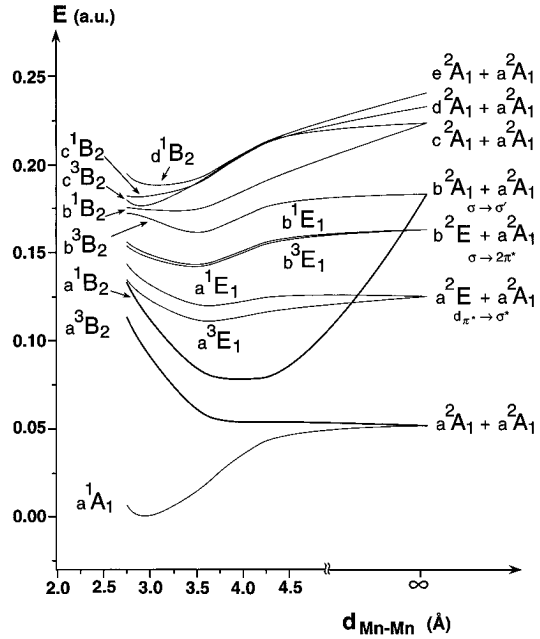

Figure 2. Potential energy curves for the metal−metal bond homolysis in $Mn_2(CO)_{10}$.

In order to locate possible photoactive states in the high-energy region of the spectrum, we have computed the potential energy curves for the $^{1,3}B_2$ and $^{1,3}E_1$ (these are the only symmetry allowed excitations in D_{4d} symmetry) excited states up to the d^1B_2 ($\sigma \rightarrow \sigma'^*$), which is the highest state that may play a role in the Mn−Mn photodissociation, given the Mn−Mn bonding and antibonding characters respectively of the σ and σ'^* orbitals. A selection of these curves is reported in Figure 2 (for clarity, six E_1 curves in this energy range have been omitted).

The a^1A_1 ground state potential energy curve is rather flat near the minimum (see Figure 2), a feature also present in the potential curve computed by Veillard and Rhomer[64] by configuration interaction (CI) calculations.

As expected, the a^3B_2 potential energy curve corresponding to the $\sigma \rightarrow \sigma^*$ excitation is strongly dissociative with respect to the Mn−Mn bond. The molecule will dissociate along this curve to the $Mn(CO)_5$ radicals in their $^2A_1$ ground states. According to the experimental findings,[14] recombination of the two $Mn(CO)_5$ radicals to form $Mn_2(CO)_{10}$ will then easily occur along the ground state potential energy curve.

The corresponding a^1B_2 potential energy curve shows a shallow minimum at a very large Mn−Mn distance (around 4 Å), indicating that the a^1B_2 is a bound state, although the metal−metal bond is considerably weakened. Note that the a^1B_2 curve between 4.5 Å and ∞ is just sketched, since no points at these large distances have been calculated. If the a^1B_2 state would correspond to a $\sigma \rightarrow \sigma^*$ excitation between the bonding and antibonding orbitals of a simple electron pair bond, a minimum in the a^1B_2 curve would be expected and the dissociation would lead to $Mn(CO)_5^+$ and $Mn(CO)_5^-$ moieties. However, although the triplet and singlet states arising from the $\sigma \rightarrow \sigma^*$ excitation

(51) Folga, E.; Ziegler, T. *J. Am. Chem. Soc.* **1993**, *115*, 5169.
(52) Almenningen, A.; Jacobsen, G. G.; Seip, H. M. *Acta Chem. Scand.* **1969**, *23*, 685.
(53) Dahl, L. F. ; Rundle, R. E. *Acta Crystallogr.* **1963**, *16*, 419.
(54) Martin, M.; Rees, B.; Mitschler, A. *Acta Crystallogr.* **1982**, *B38*, 6.
(55) Simões, M.; Beauchamp, J. L. *Chem. Rev.* **1990**, *90*, 629.
(56) Junk, G. A.; Svec, H. J. *J. Chem. Soc. A* **1970**, 2102.
(57) Bidinosti, D. R.; McIntyre, N. S. *Can. J. Chem.* **1970**, *48*, 593.
(58) Connor, J. A.; Zafarani-Moattar, M. T.; Bickerton, J.; El Saied, N. I.; Suradi, S.; Carson, R.; Al-Takhin, G.; Skinner, H. A. *Organometallics* **1982**, *1*, 1166.
(59) Marcomini, A.; Poë, A. *J. Am. Chem. Soc.* **1983**, *105*, 6952.
(60) Marcomini, A.; Poë, A. *J. Am. Chem. Soc., Dalton Trans.* **1984**, 95.
(61) Simões, M.; Beauchamp, J. L. *Organometallics* **1985**, *4*, 1238.
(62) Goodman, J. L.; Peters, K. S.; Vaida, V. *Organometallics* **1986**, *5*, 815.
(63) Smith, G. P. *Polyhedron* **1988**, *7*, 1605.
(64) Veillard, A.; Rhomer, M.-M. *Int. J. Quantum Chem.* **1992**, *42*, 965.

behave largely as expected for a prototype electron pair bond, the singlet excited state does not asymptotically go to ions since it will change through an avoided crossing (not drawn in the figure) to the obviously much lower $^1B_2$ state arising from one $Mn(CO)_5$ in its b^2A_1 excited state and the other one in its a^2A_1 ground state.

The $a^{1,3}E_1$ potential energy curves corresponding to the $d_{\pi^*} \rightarrow \sigma^*$ ($8e_3 \rightarrow 10b_2$) excitation are weakly dissociative, although they show a very shallow minimum around 3.50 Å. This implies that both $d_{\pi^*} \rightarrow \sigma^*$ and $\sigma \rightarrow \sigma^*$ excitations may lead to Mn−Mn cleavage. An interesting feature shown by the potential energy curves reported in Figure 2 is the close proximity of the a^3E_1 and a^1B_2 PECs near the Mn−Mn equilibrium distance. We will see below that this feature has some relevance in the explanation of the concomitant Mn−Mn and Mn−CO bond photodissociation at low energy.

Coming now to the higher energy excited states, the $^{1,3}E_1$ states from b upward are not photoactive with respect to Mn−Mn cleavage, although most of them correspond to excitations which depopulate the σ orbital. This is the case, for instance, for the $b^{1,3}E_1$ ($\sigma \rightarrow 2\pi^*$) states whose PECs are shown in Figure 2. Comparing the behavior of the $b^{1,3}E_1$ states, which correspond to depopulation of the Mn−Mn σ-bonding orbital, with that of the $a^{1,3}E_1$ states, which correspond to population of the Mn−Mn σ-antibonding orbital, suggests that depopulation of the σ-bonding orbital has a less detrimental effect on the Mn−Mn bond than population of the Mn−Mn antibonding σ^* orbital, which in the case of the $a^{1,3}E_1$ states is by itself sufficient to break the bond.

As for the high-energy $^3B_2$ and $^1B_2$ states, these are not dissociative, although the b^3B_2 is barely bound indeed. The c^3B_2 and d^1B_2 correspond at the equilibrium distance to $\sigma \rightarrow \sigma'^*$ excitations. The triplet $\sigma \rightarrow \sigma'^*$ excited state moves through an avoided crossing from the c^3B_2 to the b^3B_2 state around 3.0 Å. Beyond this distance the b^3B_2 PEC corresponds to the $\sigma \rightarrow \sigma'^*$ excitation. Although it is not visible in the features of the PECs (more points would be required to resolve such detail), the singlet $\sigma \rightarrow \sigma'^*$ excited state traverses through avoided crossings from the d^1B_2 PEC to the c^1B_2 and b^1B_2 states between the equilibrium distance and 3.5 Å. At 3.5 Å the b^1B_2 state corresponds to the $\sigma \rightarrow \sigma'^*$ excitation.

Clearly high-energy symmetry allowed excitation into one of the b,c,d^1B_2 states does not bring the system into a photoactive state with respect to Mn−Mn bond dissociation. A possible mechanism for Mn−Mn bond dissociation, which will have to compete with Mn−CO bond breaking (see below), would consist of the molecule reaching through intersystem crossing the c^3B_2 and dissociating after crossing to a vibrationally excited b^3B_2 state. Such crossings may take place more efficiently in solution than in the gas phase. As a matter of fact, gas-phase photoexperiments indicate that excitation at $\lambda \leq 248$ nm (the calculated excitation energy to d^1B_2 is 249 nm) only leads to CO loss,[15] while solution photoexperiments indicate that excitation at $\lambda \leq 266$ nm leads to both processes, CO loss and Mn−Mn cleavage,[5−14] although the quantum yield of the latter is very low.

Photodissociation of a Carbonyl Ligand

As already mentioned, it is well-established that $Mn_2(CO)_9$ is the primary photoproduct following the loss of a carbonyl ligand, be it axial or equatorial. Since this is a transient species, informations regarding its structure have only been indirect, although matrix isolation experiments have been interpreted in terms of a linear semibridged structure.[8,11] The only available calculations concerning the structure of $Mn_2(CO)_9$ were performed by Veillard and Rhomer,[64] using *ab initio* methods. Four different structures have been investigated by these authors: two purely metal−metal bonded structures of C_{4v} and C_s symmetry corresponding to the departure of one axial and respectively of one equatorial ligand from $Mn_2(CO)_{10}$, one dissymmetric structure of C_s symmetry with a semibridging carbonyl, and one symmetric with a classical CO bridge, of C_{2v} symmetry. The authors however note some limitations of these calculations, in particular the use of fixed geometries. In order to get a more reliable evaluation of their relative stabilities, geometry optimization of these structures would be required. With this aim we have reinvestigated the structures proposed by Veillard and Rhomer as the most likely for $Mn_2(CO)_9$, including a purely metal−metal bonded structure, of C_s symmetry, with an equatorial vacancy and in the eclipsed configuration. This is also a possible structure for $Mn_2(CO)_9$ following the loss of an equatorial carbonyl from $Mn_2(CO)_{10}$. We have not attempted any calculation for the structure with a classical CO bridge since, according to the Veillard and Rhomer calculations,[64] it is much higher in energy than the other ones. Similarly, structures with several bridging carbonyls have not been considered in this study. The optimized geometries for the investigated $Mn_2(CO)_9$ structures are reported in Figure 3.

All of these structures have a closed-shell ground state. From our calculations the structure with a semibridging carbonyl group $Mn_2(CO)_8(\mu\text{-}\eta^1\text{:}\eta^2\text{-CO})$ is the lowest in energy, in agreement with the experimental findings,[8,11] but in disagreement with CI calculations by Veillard and Rhomer[64] that give the linear semibridged structure as much less stable than the two purely metal−metal bonded C_{4v} (with an axial vacancy) and C_s (with an equatorial vacancy) structures. This discrepancy might be due to the fact that in the CI calculations the structures were not allowed to relax.

Concerning the relative stabilities of the different structures of $Mn_2(CO)_9$, we note that, compared to the linear semibridged structure, the staggered conformation of $Mn_2(CO)_9$ with an equatorial vacancy (Figure 3b) is only 12 kJ mol^{-1} less stable, while the eclipsed one (Figure 3c) is much higher in energy (41 kJ mol^{-1}), indicating that the rotation barrier between these two conformations is not negligible. Furthermore, the energies of the purely metal−metal bonded structures of $Mn_2(CO)_9$ corresponding respectively to the departure of one axial and of one equatorial ligand from $Mn_2(CO)_{10}$ (Figure 3a,b) differ by 23 kJ mol^{-1}, where Veillard and Rhomer[64] find an energy difference of only 3 kJ mol^{-1}.

Although our calculations indicate the semibridged structure as the most stable one for $Mn_2(CO)_9$, one should remember that it is not a primary photoproduct. As we have already pointed out, this species is formed via secondary photolysis of a solvent compound, $Mn_2(CO)_9$(solv) (where solv represents a solvent molecule), which is clearly the prominent initial product following CO loss from $Mn_2(CO)_{10}$.[12,38,39] The rate constant and the enthalpy of activation for semibridge formation from the solvent species have been recently estimated by Zhang *et al.*[12] to be 1×10^6 s^{-1} and ~21 kJ mol^{-1}, respectively. It seems quite reasonable then to consider as primary photoproducts following CO loss the purely metal−metal bonded structures of $Mn_2(CO)_9$, corresponding to the departure of one axial (see Figure 3a) or of one equatorial ligand (see Figure 3b), rather than the most stable semibridged structure. In fact the coordinatively unsatured structures with an axial or an equatorial vacancy are the most likely precursors of the solvento species, being suitable for reaction with solvent molecules. Unfortunately, gas-phase experiments available to date do not give any indication about the structure of $Mn_2(CO)_9$ following CO loss.

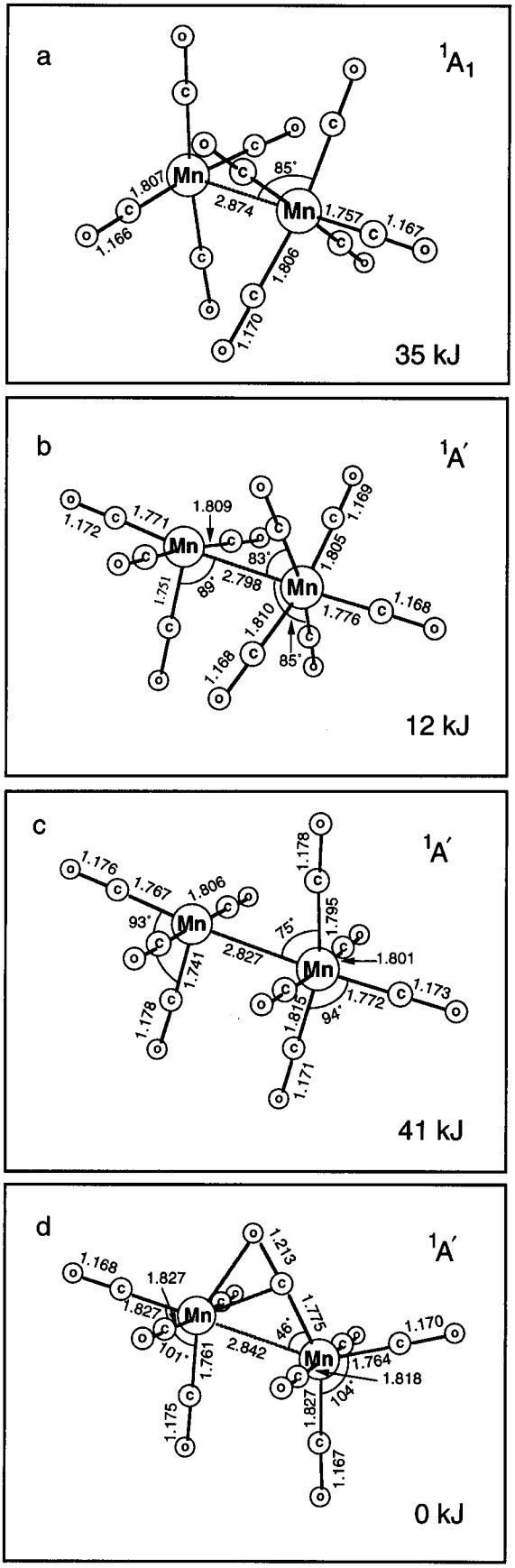

Figure 3. Optimized structures for $Mn_2(CO)_9$ in (a) C_{4v} symmetry with an axial vacancy; (b) C_s symmetry with an equatorial vacancy, in the staggered configuration; (c) C_s symmetry with an equatorial vacancy, in the eclipsed configuration; (d) C_s symmetry with a semibridging carbonyl group. All energies are with respect to the semibridged species geometry of (d), which has the lowest energy.

We have computed, using different theoretical DF models, the energetics of the process $Mn_2(CO)_{10} \rightarrow Mn_2(CO)_9 + CO$ considering $Mn_2(CO)_9$ in the purely metal−metal bonded structures mentioned above and, for comparison purposes, in the semibridged structure. The energy values, referred to as ΔH_{ax}, ΔH_{eq}, and ΔH_{sb}, respectively, are reported in Table 1 and compared to the only available first carbonyl ligand dissociation enthalpy of $Mn_2(CO)_{10}$.[63,65] As expected, on the basis of the relative stabilities of the $Mn_2(CO)_9$ structures, the dissociation of an axial carbonyl requires more energy compared to the dissociation of an equatorial carbonyl.

Again it is found that adding the nonlocal exchange and correlation corrections to the LSDA energy expression improves considerably the agreement between theory and experiment. The ΔH_{ax} and ΔH_{eq} computed using the nonlocal exchange and correlation corrections are in reasonable agreement with the experimental datum, although the best value is obtained considering $Mn_2(CO)_9$ in its most stable configuration. The relative stabilities of the reactant and the products corresponding both to axial and equatorial CO loss are correctly reproduced by our calculations, and this assures that the potential energy curves for the loss of a carbonyl ligand will have the right slope.

Potential Energy Curves for the Loss of an Axial Carbonyl Ligand. Before discussing the features of the PEC for the dissociation of a carbonyl ligand, it is useful to look at the level scheme of Figure 4 that we have constructed in order to follow the evolution of the $Mn_2(CO)_{10}$ MOs on elongating the Mn−CO_{ax} bond to the dissociation limit. As far as the highest occupied levels are concerned, we note that, upon the lengthening of the Mn−CO_{ax} bond, the $10a_1$-σ ($19a_1$ in C_{4v} symmetry) level remains almost unchanged, while the $8e_3$-d_{π^*} ($16e_1$ in C_{4v} symmetry) is destabilized and becomes the highest occupied orbital when the Mn−CO_{ax} distance is 2.5 Å. This is understandable in view of the negligible CO_{ax} participation to the $10a_1$-σ and the Mn−CO_{ax} π bonding character of the $8e_3$-d_{π^*} (we refer to ref 16 for a detailed discussion of the characteristics of the various occupied and virtual orbitals).

The most interesting features of the scheme of Figure 4 are however concerned with the behavior of some virtual levels, namely, $10b_2$-σ^*, the $11a_1$-σ', and $11b_2$-σ'^* (for clarity, the virtual levels $9e_3$, $7e_2$, $9e_1$, $10e_1$, $8e_2$, $10e_3$, and $11e_1$, which are located in the −3 to −4 eV range and are insensitive to the Mn−CO_{ax} bond distance, are not shown). The σ' levels have much d_{z^2} character and are strongly antibonding with the axial COs:[16] $\sigma'(\sigma'^*) \sim (d^1_{z^2} \pm d^2_{z^2}) - (5\sigma^1 \pm 5\sigma^2)$, where the minus sign refers to σ'^*, the superscripts 1 and 2 refer to the left and right side of $Mn_2(CO)_{10}$, respectively. Note that the axial CO is leaving from the left side. As soon as the axial CO moves away, the symmetry of the system lowers and the $11a_1$-σ' and $11b_2$-σ'^* mix and form the $\sigma' + \sigma'^*$ and $\sigma' - \sigma'^*$ combinations corresponding to the $21a_1$ and the $22a_1$ C_{4v} orbitals. The first localizes on the side where CO is leaving ($d^1_{z^2} - 5\sigma^1$), the second localizes on the other side ($d^2_{z^2} - 5\sigma^2$). Owing to the strong Mn−CO_{ax} σ-antibonding character of the σ' orbitals, the $21a_1$ is downward shifted upon the lengthening of the Mn−CO_{ax} bond; the $22a_1$ is not. Around 2.1 Å the $21a_1$-($\sigma' + \sigma'^*$) starts to mix with the $20a_1$-σ^*, and at 2.5 Å, the $20a_1$ has become mostly $\sigma' + \sigma'^*$ and the $21a_1$ has acquired much σ^* character. In other words, in the range 2.1−2.5 Å these orbitals exhibit an (avoided) crossing. This will have important consequences for the lowest excited states. For instance, the lowest excited state of $Mn_2(CO)_9$ with an axial vacancy will be the ^3E state resulting from $16e \rightarrow 20a_1(\sigma' + \sigma'^*)$ excitation. At equilibrium

(65) Lewis, K. E.; Golden, D. M.; Smith, G. P. *J. Am. Chem. Soc.* **1983**, *105*, 6952.

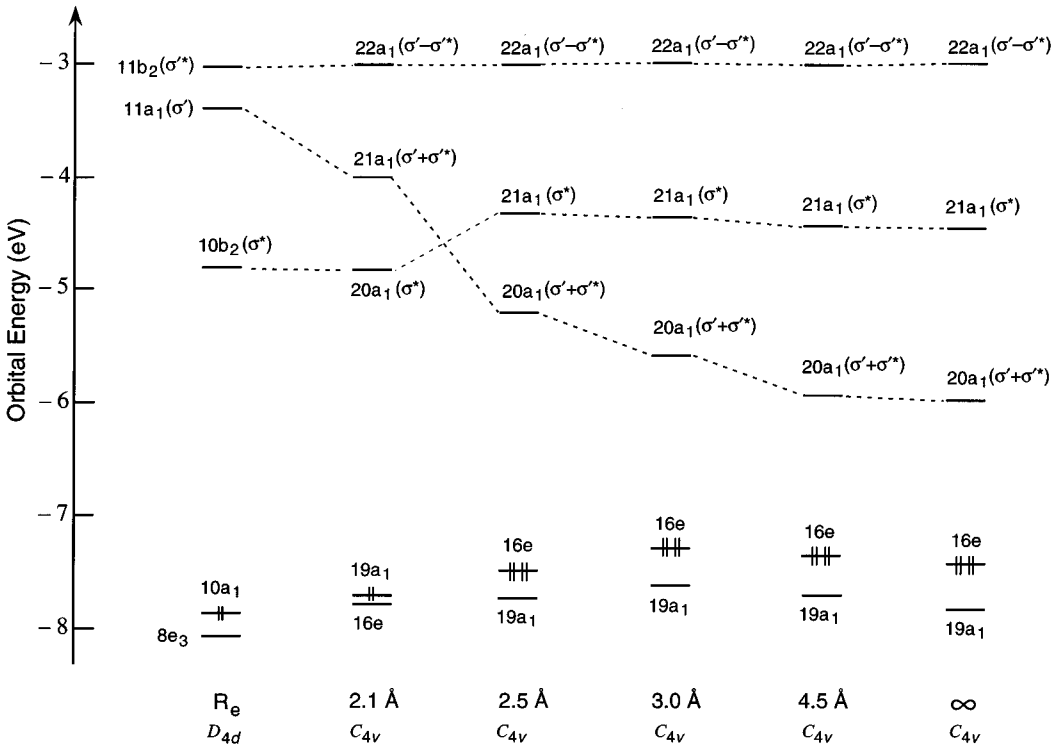

Figure 4. Evolution of the highest occupied and lowest unoccupied MOs of $Mn_2(CO)_{10}$ for an increase of the $Mn-CO_{ax}$ bond length to the dissociation limit. Since there are no axial CO orbitals which transform according to E_2 symmetry, the e (C_{4v}) e_2-derived levels are not shown in the scheme.

geometry (of $Mn_2(CO)_{10}$) the E state corresponding to $d_{\pi^*} \rightarrow \sigma'$ excitation ($8e_3 \rightarrow 11a_1$) will be high lying, but it will rapidly become lower in energy and it will, after a number of avoided crossings with lower E states in the range 2.1−2.5 Å, eventually cross the $d_{\pi^*} \rightarrow \sigma^*$ excited state, which at equilibrium distance is the lowest one of E symmetry ($8e_3$-$d_{\pi^*} \rightarrow 10b_2$-$\sigma^*$). A similar situation arises in A_1 symmetry (in C_{4v}). The lowest excited state at equilibrium geometry corresponds to $\sigma \rightarrow \sigma^*$ excitation, but this state will be crossed by the $\sigma \rightarrow (\sigma' + \sigma'^*)$ excitation, which will asymptotically be the lowest excited state of A_1 symmetry.

The implication is that even if the lowest excited states of $Mn_2(CO)_{10}$ of $\sigma \rightarrow \sigma^*$ and $d_{\pi^*} \rightarrow \sigma^*$ character are not dissociative with respect to the $Mn-CO_{ax}$ bond, as a consequence of the lack of $Mn-CO_{ax}$ antibonding in the σ^* orbital, photodissociation of an axial carbonyl ligand might still occur by curve crossing with the above mentioned $Mn-CO_{ax}$ dissociative states. Crucial questions are of course whether the asymptotic energy is not higher than the $\sigma \rightarrow \sigma^*$ and $d_{\pi^*} \rightarrow \sigma^*$ excited state energies at equilibrium geometry and if the avoided crossing does not lead to a high barrier.

The above suggestions have been checked out through the calculation of the potential energy curves for a number of $^{1,3}E$ excited states, viz., all those lying below the $^{1,3}E$ states that correspond at the equilibrium distance to the symmetry forbidden $d_{\pi^*} \rightarrow \sigma'$ ($8e_3 \rightarrow 11a_1$) $^1E_3$ state (the symmetry allowed analogue $d_\pi \rightarrow \sigma'$ ($8e_1 \rightarrow 11a_1$) m^1E_1 state lies at much higher energy). The PECs for the lowest $^{1,3}A_1$ excited states corresponding to $\sigma \rightarrow \sigma^*$ excitation have also been computed. The potential energy curves corresponding to the loss of an axial CO are displayed in Figure 5.

From Figure 5, the bound nature (with respect to $Mn-CO_{ax}$ bonding) of the $\sigma \rightarrow \sigma^*$ a^3A_1 (a^3B_2 in D_{4d} symmetry) is apparent. That this state, which is responsible for the Mn−Mn cleavage, is bonding with respect to an axial carbonyl, is in line with the negligible axial CO character of both σ and σ^* orbitals. We

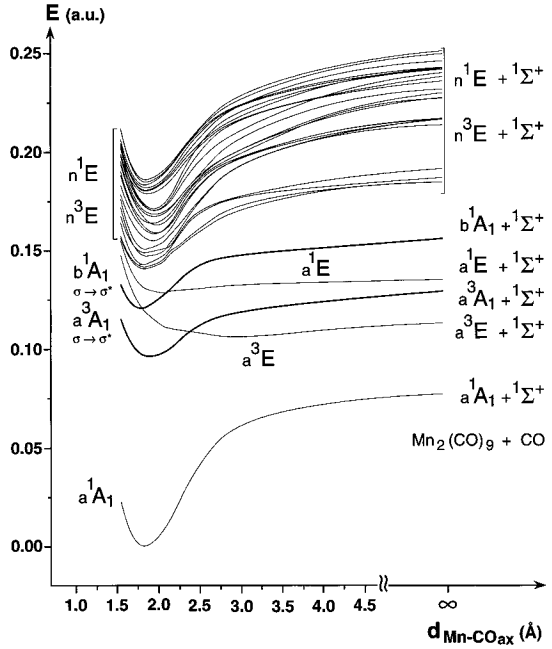

Figure 5. Potential energy curves for the dissociation of the $Mn-CO_{ax}$ bond in $Mn_2(CO)_{10}$.

note nevertheless that the well depth of the a^3A_1 curve is much less than that of the a^1A_1 ground state curve. This is due to the fact that this state does not connect to the $\sigma \rightarrow \sigma^*$ excitation ($19a_1 \rightarrow 21a_1$) in $Mn_2(CO)_9$ but becomes asymptotically the $\sigma \rightarrow (\sigma' + \sigma'^*)$ excitation ($19a_1 \rightarrow 20a_1$) in $Mn_2(CO)_9$, which has much lower excitation energy than the $\sigma \rightarrow \sigma^*$ excitation. This crossing to the $\sigma \rightarrow (\sigma' + \sigma'^*)$ excited state does not seem to involve a barrier.

In contrast to the behavior of the A_1 states, the $a^{1,3}E$ states corresponding to ($8e_3 \rightarrow 10b_2$) $d_{\pi^*} \rightarrow \sigma^*$ excitation are dissociative with respect to axial CO loss. One would not expect

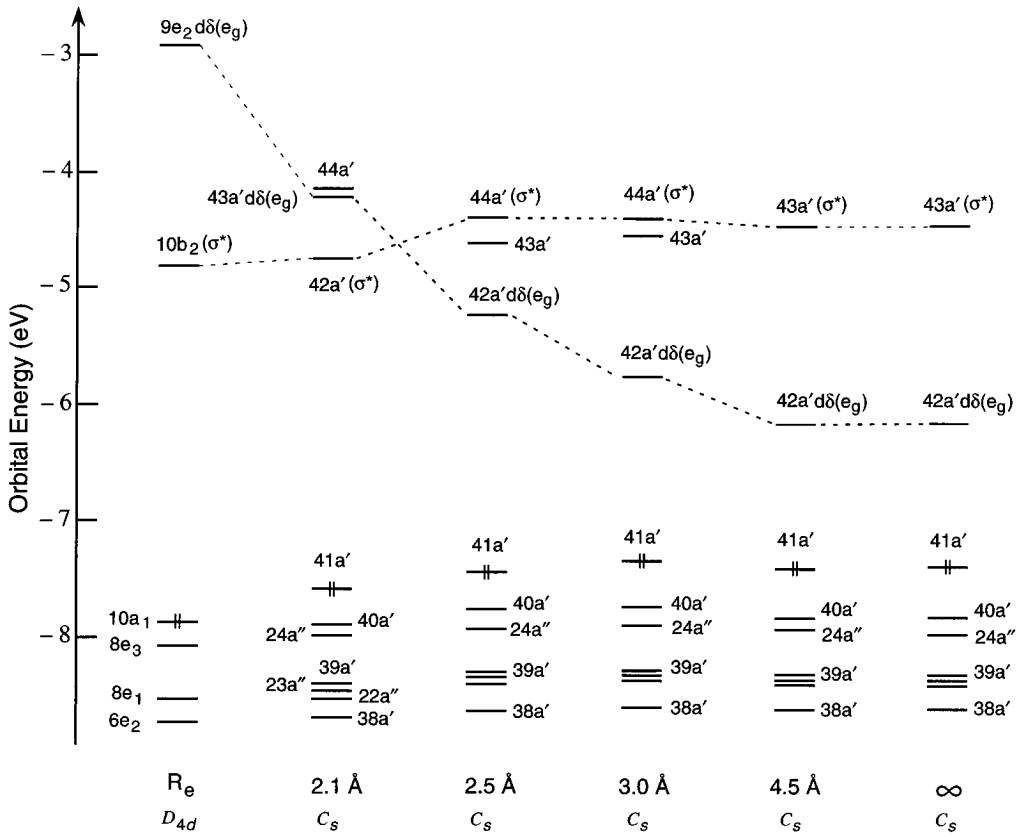

Figure 6. Evolution of the highest occupied and lowest unoccupied MOs of $Mn_2(CO)_{10}$ for an increase of the $Mn-CO_{eq}$ bond length to the dissociation limit.

this behavior on the basis of the π-bonding character of d_{π^*} (there are still three π-bonding electrons left in the $8e_3$-d_{π^*} orbitals), although some bond lengthening (more than for $\sigma \rightarrow \sigma^*$ excitation) could be expected. However, the upward shift of the $8e_3$-16e orbital due to the loss of π-bonding character, which makes the a^3E state, which is higher than a^3A_1 at equilibrium geometry, lower in $Mn_2(CO)_9$, makes a crucial difference in that it puts the asymptotic energy at about the same height as the "intended" minimum in the a^3E curve. A second important factor, which apparently prevents the occurrence of any barrier, is the very rapid lowering in energy of the $d_{\pi^*} \rightarrow \sigma'$ excited state upon $Mn-CO_{ax}$ bond lenghtening, which is completely in line with the strong d_{z^2}-$5\sigma_{ax}$ antibonding in the σ' that we stressed before.[16] It is worth noting that from 2.2 Å upward the $a^{1,3}E$ PEC corresponds to a $d_{\pi^*} \rightarrow \sigma'$ excitation, indicating that an "avoided crossing" with the LF dissociative state derived from $(8e_3 \rightarrow 11a_1)d_{\pi^*} \rightarrow \sigma'$ excitation has already occurred at this short distance. (d_{π^*} and σ' in this paragraph actually stand for the appropriate localized orbitals, *vide supra*). The lack of an energy barrier in the a^3E PEC due to the avoided crossing may be "explained" as being caused by the precipitous lowering of the $d_{\pi^*} \rightarrow \sigma'$ excitation, overtaking the $d_{\pi^*} \rightarrow \sigma^*$ excitation before it has had time to curve upward. We have investigated the a^3E PEC more closely between 2.1 and 2.5 Å by calculating the curve at a finer grid of distances, but no energy barrier has been found. The rapid descent of $d_{\pi^*} \rightarrow \sigma'$ character can be traced through the multitude of excited states shown in the figure: at 1.6 Å the highest ^3E state in the figure is $d_{\pi^*} \rightarrow \sigma'$; at 2.2 Å the lowest ($a^3E$) has this character. We conclude that we have been able to identify possible CO_{ax} loss mechanisms in the low-lying excited states (the $d_{\pi^*} \rightarrow \sigma^*$ excited states) of $Mn_2(CO)_{10}$. The dissociative nature of the corresponding PECs is basically due to the rapid lowering of the $Mn(3d_{z^2})-CO_{ax}(5\sigma)$ antibonding $\sigma' + \sigma'^*$ orbital upon $Mn-CO_{ax}$ bond lengthening. This causes the first excitation energies in $Mn_2(CO)_9$ to be much lower than in $Mn_2(CO)_{10}$, which compensates for the Mn−CO bond breaking energy and puts the first excited states of the $Mn_2(CO)_9$ + dissociated CO system at about the same energy as the first excited states of $Mn_2(CO)_{10}$. This picture of the axial CO dissociation is in excellent agreement with deductions from very recent time-resolved experiments.[39] We note that axial CO dissociation may not only occur in the a^1E state but also by an intersystem crossing from the b^1A_1 to the a^3E state. This is important since irradiation into the $\sigma \rightarrow \sigma^*$ band will heavily populate b^1A_1. Mn−Mn and $Mn-CO_{ax}$ bond breaking will result from different intersystem crossings from the b^1A_1 to dissociative triplet states, one to the a^3A_1 (=a^3B_2 in D_{4d} symmetry), the other one to a^3E. These processes may therefore be competitive. We caution that our calculations probably have some inaccuracy in the relative energies of the b^1A_1 and a^1E energies and therefore in the point of crossing of b^1A_1 with a^3E. The intense first band in the UV spectrum most probably corresponds to the b^1A_1 and the low-energy shoulder of this band to the a^1E. This means that a^3E and a^1E should be somewhat downshifted with respect to the $\sigma \rightarrow \sigma^*$ states.

Potential Energy Curves for the Loss of an Equatorial Carbonyl Ligand. A first step in the understanding of the photodissociation mechanism of an equatorial carbonyl ligand is again provided by a level scheme (Figure 6) that illustrates the evolution of the highest occupied and lowest unoccupied $Mn_2(CO)_{10}$ MOs on elongating the $Mn-CO_{eq}$ bond to the dissociation limit. Note that the leaving CO is along the *x*-axis, the Mn−Mn bond being the *z*-axis. π-Bonding will therefore be lost with a d_π orbital on Mn^1 (d^1_{xz}) and a d_δ orbital on Mn^1 (d^1_{xy}).

As for the highest occupied levels, one will notice that, unlike in the case of $Mn-CO_{ax}$ bond elongation, the $10a_1$-σ orbital ($41a'$ in C_s symmetry) is destabilized by the lengthening of the

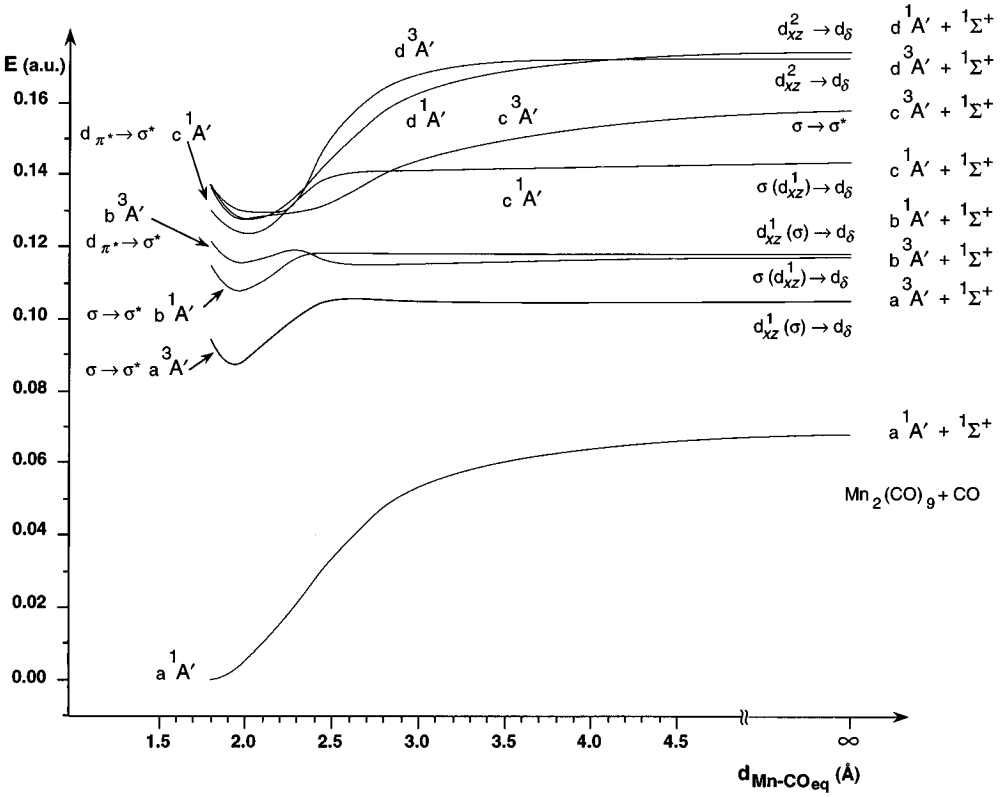

Figure 7. $^{1,3}A'$ potential energy curves for the dissociation of the $Mn-CO_{eq}$ bond in $Mn_2(CO)_{10}$.

$Mn-CO_{eq}$ bond. This is in line with the $Mn-CO_{eq}$ π-bonding character of this orbital (through the involvement of $4p_z$; see ref 16).

The $8e_1$-d_π, $8e_3$-d_{π^*} orbitals are, upon $D_{4d} \rightarrow C_s$ symmetry lowering, split into two sets, 39a′, 23a″ and 40a′, 24a″, respectively. The a′ levels are d^1_{xz} and d^2_{xz}; the first is destabilized for increasing $Mn-CO_{eq}$ bond length due to the loss of $Mn-CO_{eq}$ π-bonding character and becomes 40a′. In C_s symmetry the two degenerate components of the $6e_2$-$d_\delta(t_{2g})$ orbital, $d^1_{xy} + d^2_{x^2-y^2}$ and $d^1_{xy} - d^2_{x^2-y^2}$, mix to form localized 22a″ and 38a′ orbitals. The former has d^1_{xy} character; the latter has $d^2_{x^2-y^2}$ character. As we are moving an equatorial carbonyl bonded to the manganese atom on the left (see Figure 1 and Scheme 3), the 22a″-d^1_{xy} is destabilized upon elongation of the $Mn-CO_{eq}$ bond; the 38a′-$d^2_{x^2-y^2}$ stays put.

Turning now to the virtual levels, the level scheme of Figure 6 displays a situation somewhat similar to that of Figure 4. Again a high-lying level is strongly downward shifted by $Mn-CO_{eq}$ bond lengthening. It is the a′ component of the $9e_2$-$d_\delta(e_g)$ degenerate set consisting of (combinations of) $d^1_{x^2-y^2}$ and d^2_{xy} that are strongly antibonding with the 5σ's of the equatorial carbonyls. Upon $D_{4d} \rightarrow C_s$ symmetry lowering the two $d^2_{xy} + d^1_{x^2-y^2}$ and $d^2_{xy} - d^1_{x^2-y^2}$ components of the $9e_2$-$d_\delta(e_g)$ mix to form the localized d^2_{xy} and $d^1_{x^2-y^2}$ orbitals. d^2_{xy} is of course not affected by the departure of an equatorial CO from the left Mn. At a $Mn-CO_{eq}$ distance of about 2.1 Å $d^1_{x^2-y^2}$ has descended from its position as 52a′ to become 43a′, and at 2.5 Å, σ^* and $d^1_{x^2-y^2}$ have crossed and the σ^* character is mostly in 44a′ and subsequently in 43a′, while 42a′ has become largely $d^1_{x^2-y^2}$. In fact, in 42a′ $d^1_{x^2-y^2}$ hybridizes strongly with $4p_x$ to reduce the antibonding with the CO at the negative x-axis, which of course helps to lower the orbital energy. In comparison to the behavior of the $6e_2$-$d_\delta(t_{2g})$ derived set of orbitals, it is clear that the loss of σ-antibonding in $9e_2$-$d_\delta(e_g)$ has much more effect than the loss of π-bonding with the d^1_{xy} orbital of the $6e_2$-$d_\delta(t_{2g})$ set. The consequence of the downward shift of the $d_\delta(e_g)$-$d^1_{x^2-y^2}$ is that asymptotically the lowest excited states will correspond to excitations from the occupied d's to this orbital. The high-lying A′ and A″ excited states resulting from excitations to $9e_2$-$d_\delta(e_g)$-$d^1_{x^2-y^2}$ at equilibrium geometry will therefore after a number of avoided crossings with lower A′ (A″) states in the range 2.1−2.5 Å, become the lowest A′ (A″) states. It follows that photodissociation of an equatorial carbonyl ligand at low energy might occur from the $a^{1,3}B_2$ ($\sigma \rightarrow \sigma^*$) or $a^{1,3}E_1$ ($d_\pi^* \rightarrow \sigma^*$) states if their PECs are crossed by the above mentioned $Mn-CO_{eq}$ dissociative excited states, provided that the avoided crossings do not lead to high-energy barriers.

In order to verify the occurrence of the avoided crossings predicted so far, we have explicitly calculated the potential energy curves for the lowest three $^{1,3}A'$ and $^{1,3}A''$ excited states. These PECs are displayed in Figures 7 and 9 for A′ and A″ symmetries separately. Considering first the A′ excited states, it is noted that the a^3A' that corresponds at the equilibrium distance to the $\sigma \rightarrow \sigma^*$ excitation ($^3B_2$) which is responsible for the Mn−Mn cleavage does not show $Mn-CO_{eq}$ dissociative character. The corresponding singlet b^1A' PEC has similar behavior. However, it is clear that the well depth of these excited state PECs is much smaller than that of the ground state a^1A'. This is, of course, as in the case of $Mn-CO_{ax}$ dissociation, due to the much lower first excitation energy in $Mn_2(CO)_9$ than in $Mn_2(CO)_{10}$ at the equilibrium geometry, which in turn is mostly due to the lowering of the $d_\delta(e_g)$-$d^1_{x^2-y^2}$ orbital. The next higher excited triplet state, b^3A', corresponding at the equilibrium distance to $d_\pi^* \rightarrow \sigma^*$ excitation ($^3E_1$), is weakly dissociative with respect to CO loss, after going over a barrier around 2.3 Å. The remaining PECs do not exhibit any dissociative character. We have mentioned the change in character of the lowest excited states along the $Mn-CO_{eq}$ coordinate, due to the LUMO changing from σ^* to $d_\delta(e_g)$-$d^1_{x^2-y^2}$. The difference in character between the low-lying excitations in $Mn_2(CO)_{10}$ at equilibrium geometry and in Mn_2-

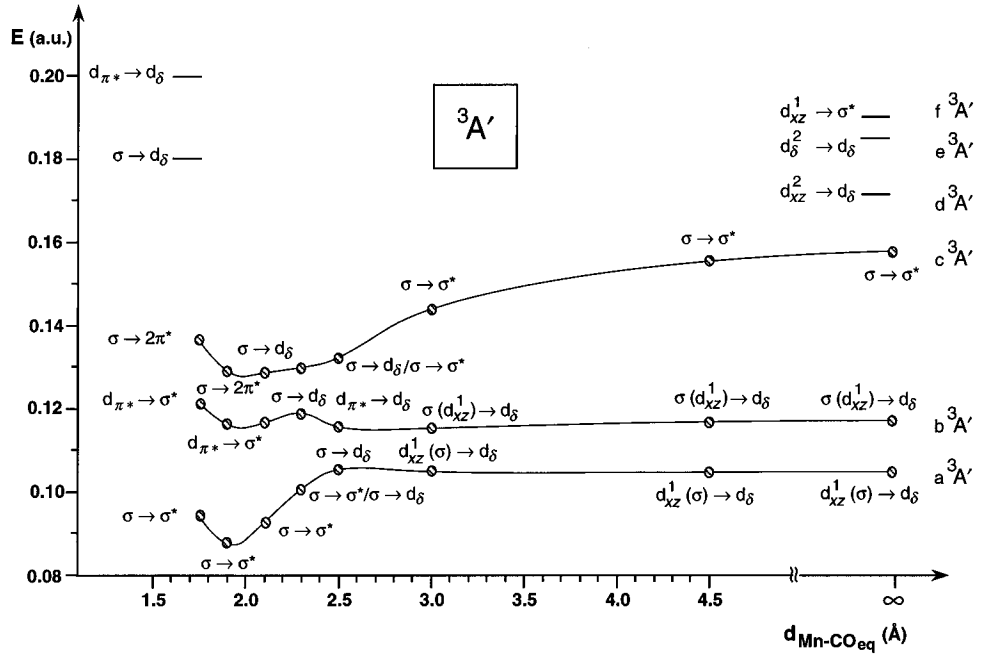

Figure 8. $^3A'$ potential energy curves for the dissociation of the $Mn-CO_{eq}$ bond in $Mn_2(CO)_{10}$. The dominant character of the states along the photodissociation pathway is emphasized. On the left top are indicated the energies of the high-lying LF $^3A'$ photoactive states at the equilibrium distance. Their corresponding energies at the dissociation limit are indicated on the right side.

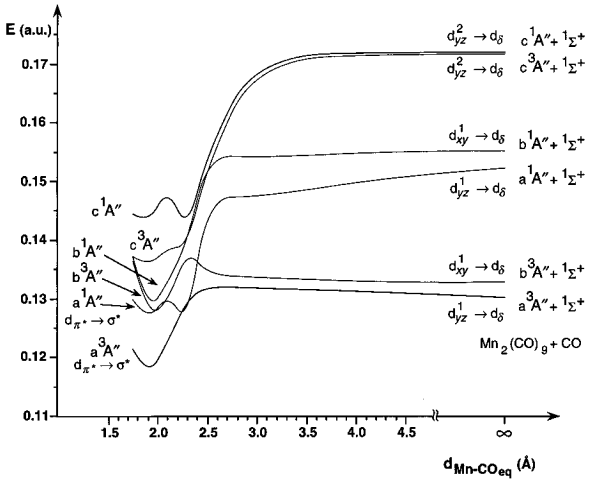

Figure 9. $^{1,3}A''$ potential energy curves for the dissociation of the $Mn-CO_{eq}$ bond in $Mn_2(CO)_{10}$.

$(CO)_9$ implies the presence of avoided crossings, or at least a switching of the orbital type of excitation, between the PECs in the region 2.1−3.0 Å. The nature of the A′ excited states is illustrated in detail for the lowest a^3A', b^3A', and c^3A' excited states in Figure 8. The excitations to d_δ (we further denote the $d_\delta(e_g)$-$d^1_{x^2-y^2}$ orbital as just d_δ) are at high energy at the equilibrium geometry but rapidly become lower in energy and end up as the lowest excitations in $Mn_2(CO)_9$. a^3A', which corresponds to $\sigma \rightarrow \sigma^*$ excitation up to 2.1 Å, acquires $\sigma \rightarrow d_\delta$ and subsequently $d_\pi^* \rightarrow d_\delta$ character through crossing with the dissociative $10a_1 \rightarrow 9e_2$ ($\sigma \rightarrow d_\delta$) and $8e_3 \rightarrow 9e_2$ ($d_\pi^* \rightarrow d_\delta$) derived states. In the absence of these crossings the a^3A' PEC would asymptotically correlate with the c^3A' excited state of $\sigma \rightarrow \sigma^*$ character. Considering the nature of the a^3A' state more closely reveals that there is considerable localization of orbitals on one or the other side of the molecule, which is possible due to the symmetry lowering and which also occurs in the ground state of $Mn_2(CO)_9$. Therefore at longer $Mn-CO_{eq}$ distances the symmetrical notation such as d_π^* becomes less appropriate. In the a^3A' state the hole gains more d^1_{xz} than $d_\pi^* = d^1_{xz} + d^2_{xz}$ character. Excitations where the hole localizes on the same Mn as where the excited electron is located (i.e., Mn^1) tend to be lower in energy than excitations where the hole shows less localization (e.g., for excitation out of σ) or localizes on the other Mn. The σ orbital is built from two monomer orbitals with large overlap and does not localize readily. The d orbitals however have small overlap, and in many excited states there is a d hole that is completely localized on the left or on the right Mn. In the case of the a^3A' state we have noted that asymptotically there is still considerable $\sigma \rightarrow d_\delta$ character, but the relatively favorable hole localization on Mn^1 causes the excitation to become more $d^1_{xz} \rightarrow d_\delta$ like. This is denoted in the figure as $d^1_{xz}(\sigma) \rightarrow d_\delta$.

The b^3A' state, which corresponds at R_e to $d_\pi^* \rightarrow \sigma^*$ ($^3E_1$) excitation, also changes character in the range 2.1−2.5 Å. We are able to identify at 2.3 Å the character as $\sigma \rightarrow d_\delta$, but at 2.5 Å considerable $d_\pi^*(d^1_{xz}) \rightarrow d_\delta$ has crept in. Asymptotically b^3A' still has a hole with much σ character, i.e., can best be classified as $\sigma(d^1_{xz}) \rightarrow d_\delta$. So the b^3A' PEC has "crossed" first the dissociative $\sigma \rightarrow d_\delta$ excitation and next the dissociative $d_\pi^* \rightarrow d_\delta$ excitation. It is interesting to observe that the maximum at ∼2.3 Å in the b^3A' PEC is clearly due to an avoided crossing with the c^3A' PEC, as is apparent from the switching of $\sigma \rightarrow d_\delta$ character from c^3A' to b^3A'. The $d_\pi^* \rightarrow \sigma^*$ character of b^3A' at equilibrium geometry moves to higher PECs and ends up (as mostly $d^1_{xz} \rightarrow \sigma^*$) in the f^3A' excited state of $Mn_2(CO)_9$. The b^3A' PEC is dissociative in the sense that the asymptotic energy is lower than the energy at equilibrium geometry. The barrier due to avoided crossing is rather low (less than 10 kcal/mol).

The c^3A' PEC corresponding at the equilibrium distance to $10a_1 \rightarrow 9e_3$ ($\sigma \rightarrow 2\pi^*$) shows in the range 2.1−3.0 Å a behavior that results from interactions with other A′ states. As expected, owing to the crossing with the dissociative $10a_1 \rightarrow 9e_2$ ($\sigma \rightarrow d_\delta$) derived state, its dominant character at 2.1 Å is already $\sigma \rightarrow d_\delta$, becoming at 2.3 Å $d_\pi^* \rightarrow d_\delta$, due to crossing with the dissociative $8e_3 \rightarrow 9e_2$ ($d_\pi^* \rightarrow d_\delta$) derived state. Asymptotically c^3A' becomes the $\sigma \rightarrow \sigma^*$ of $Mn_2(CO)_9$. It is not dissociative.

With respect to higher excited states of $^3A'$ symmetry in Mn_2-

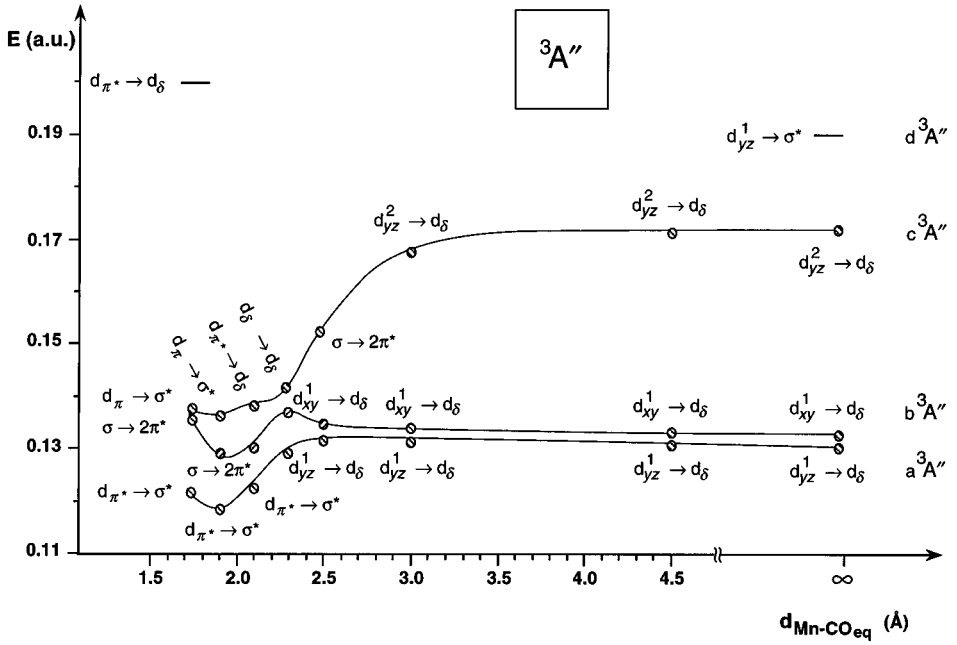

Figure 10. $^3A''$ potential energy curves for the dissociation of the Mn−CO_{eq} bond in $Mn_2(CO)_{10}$. The dominant character of the states along the photodissociation pathway is emphasized. On the left top are indicated the energies of the high-lying LF $^3A''$ photoactive states at the equilibrium distance. Their corresponding energies at the dissociation limit are indicated on the right side.

$(CO)_9$ we note that d^3A', which has $d^2_{xz} \rightarrow d_\delta$ character, is much higher than a^3A' because now the hole in d_π is on the other Mn. Similarly e^3A' has the hole in a d_δ ($d^2_{x^2-y^2}$) on the right Mn atom (see below). The charge separation that occurs in these excited states makes them higher than $\sigma \rightarrow \sigma^*$ even if this could not be expected on the basis of the orbital energy differences in Figure 6.

Turning now to the A′ singlet states (see Figure 7), b^1A' and c^1A' behave as the corresponding a^3A' and b^3A' triplets. b^1A' crosses the $10a_1 \rightarrow 9e_2$ ($\sigma \rightarrow d_\delta$) and $8e_3 \rightarrow 9e_2$ ($d_{\pi^*} \rightarrow d_\delta$) derived states and at the dissociation limit has $d^1_{xz}(\sigma) \rightarrow d_\delta$ character. c^1A' crosses the same excited states and asymptotically has $\sigma(d^1_{xz}) \rightarrow d_\delta$ character. There is a relatively large b^3A'/c^1A' triplet/singlet splitting due to the partial localization of the unpaired electrons on one manganese atom. The effect is that the c^1A' state, unlike b^3A', is not dissociative. The third singlet state, d^1A', behaves as the corresponding triplet c^3A' (i.e. has $\sigma \rightarrow 2\pi^*$ character) up to 3.0 Å, then crosses the $8e_1/8e_3 \rightarrow 9e_2$ ($d_\pi \rightarrow d_\delta$) derived state that has the hole localized on the *right* Mn atom, and asymptotically corresponds, as does the triplet d^3A', to a $d^2_{xz} \rightarrow d_\delta$ excitation. The singlet/triplet splitting is very small when the unpaired electrons are on different Mn atoms, hence, the close proximity of d^3A' and d^1A' in $Mn_2(CO)_9$.

We have now identified among the A′ states one that is Mn−CO_{eq} dissociative, namely, the $^3E_1(d_{\pi^*} \rightarrow \sigma^*)$ derived b^3A' state. We recall that the $d_{\pi^*} \rightarrow \sigma^*$ excitation is probably calculated too high with respect to the $\sigma \rightarrow \sigma^*$ excitation, so b^3A' (and c^1A') should be somewhat downshifted in Figure 7. This means, in the same way as for axial CO dissociation, that after the allowed $\sigma \rightarrow \sigma^*$ excitation to b^1A' an intersystem crossing from b^1A' to b^3A' may lead to equatorial CO dissociation. In contrast to the case of axial CO, the singlet corresponding to $d_{\pi^*} \rightarrow \sigma^*$ excitation is not dissociative for equatorial CO.

The PECs for the lowest A″ states are shown in Figures 9 and 10. From the orbital character indicated at the PECs in the asymptotic limit the various avoided crossings that must have occurred may be deduced. We do not discuss these states in detail, their behavior can be understood in much the same way as that of the A′ states. One difference is that now the $\sigma \rightarrow \sigma^*$ states are absent. The lowest state, a^3A'', corresponds at R_e to the $a^{1,3}E_1$ ($d_{\pi^*} \rightarrow \sigma^*$) state. Again the excitation will asymptotically be to d_δ; i.e., the a^3A'' changes character to become asymptotically a $d^1_{yz} \rightarrow d_\delta$ excitation, and the corresponding singlet a^1A'' has the same character. We note that d^1_{yz} is a d_π on the left Mn that is perpendicular to the leaving CO, so it does not lose π bonding with it. It is therefore less destabilized than the d^1_{xz} and the $a^3A''(d^1_{yz} \rightarrow d_\delta)$ excited state is in $Mn_2(CO)_9$ at somewhat higher energy than the states in A′ symmetry involving $d^1_{xz} \rightarrow d_\delta$ excitation, such as a^3A' and notably b^3A'. a^3A'' evolves from the same $^3E_1$ excited state at R_e as b^3A'. Whereas b^3A' has been observed to be just dissociative, in the sense that the energy at R_e is about the same as the asymptotic energy, the asymptotic energy of a^3A'' is somewhat higher (about 0.01 au, less than 10 kcal/mol), and the a^3A'' PEC is not dissociative. There is one A″ state that may be considered dissociative in the sense that its asymptotic energy is just below the energy at R_e (although not below the minimum in the curve), namely, b^3A''. b^3A'' starts at R_e as a component of $^3E_3$ ($\sigma \rightarrow 2\pi^*$). Its energy is (close to R_e) practically equal to that of $b^1A''-{}^1E_3$, also corresponding to $\sigma \rightarrow 2\pi^*$ and to that of a^1A'', i.e., $^1E_1$ ($d_\pi \rightarrow \sigma^*$). Excitations to the E_3 states are symmetry forbidden, but the b^3A'' state may become occupied by intersystem crossing from the allowed singlet excited state $a^1A''-{}^1E_1$ ($d_\pi \rightarrow \sigma^*$). It is not clear how efficient CO dissociation could be in this state since the b^3A'' PEC exhibits a clear barrier due to avoided crossing at ca. 2.3 Å, where it switches to the $d^1_{xy} \rightarrow d_\delta$ character that it will hold asymptotically. One wonders if population of the allowed $^1E_1-a^1A''$ ($d_\pi \rightarrow \sigma^*$) might, by virtue of the shape of the a^1A'' PEC, lead to CO dissociation by intersystem crossing to the a^3A'' PEC since our calculations indicate very little difference between the $^1E_1-a^1A''$ energy at equilibrium geometry and the asymptotic a^3A'' energy.

Summarizing, routes to equatorial CO dissociation along A″ PECs are less obvious than in A′ symmetry (along b^3A').

Summary

On the basis of the calculated potential energy curves the following understanding of the photochemistry of $Mn_2(CO)_{10}$ is reached. Excitation at low energy, in the experimental range of 337−355 nm will bring the molecule into $\sigma \rightarrow \sigma^*$ $^1B_2$ or into the nearly degenerate $d_{\pi^*} \rightarrow \sigma^*$ $^1E_1$ allowed excited states. From the $\sigma \rightarrow \sigma^*$ $^1B_2$ state the molecule may reach, through intersystem crossing, the corresponding $\sigma \rightarrow \sigma^*$ $^3B_2$ state which will lead to homolysis of the metal−metal bond along the $^3B_2$ curve (Figure 2), with formation of two $Mn(CO)_5$ radicals in their ground states. This is the standard explanation of the Mn−Mn bond homolysis, which is fully corroborated by our results.

For the more intriguing CO dissociation at these low excitation energies we can offer the following explanation. For the axial CO we have found the $\sigma \rightarrow \sigma^*$ $^{1,3}B_2$ states (a^3A_1,b^1A_1, Figure.5) to be bound, but the spin allowed $d_{\pi^*} \rightarrow \sigma^*$ $^1E_1$ state to be purely dissociative, leading to the products CO and $Mn_2(CO)_9$, the latter in the ^1E excited state. Also the $d_{\pi^*} \rightarrow \sigma^*$ $^3E_1$ state, that may be reached through intersystem crossing from the $d_{\pi^*} \rightarrow \sigma^*$ $^1E_1$ state or from the $\sigma \rightarrow \sigma^*$ $^1B_2$ (b^1A_1) state with which it is almost degenerate, is purely dissociative. The dissociative character of the $^{1,3}E$ curves is not due to intrinsic weakening of the $Mn-CO_{ax}$ bond upon the $d_{\pi^*} \rightarrow \sigma^*$ orbital excitation, but it is due to the strong lowering of the initially high-lying σ' orbital that rapidly localizes to the Mn^1-CO_{ax} antibonding $\sigma' + \sigma'^* = d^1_{z^2}$ ($-5\sigma^1$) orbital upon $Mn-CO_{ax}$ bond lengthening. This has the effect that the $^{1,3}E$ states change character to $d_{\pi^*} \rightarrow d^1_{z^2}$ excitation. So the $^{1,3}E$ states evolve into LF type excited states in $Mn_2(CO)_9$. However, the LF $d_{\pi^*} \rightarrow \sigma'$ excitation is initially, in $Mn_2(CO)_{10}$, much higher than the ($d_{\pi^*} \rightarrow \sigma^*$) $^{1,3}E$ states, but it comes down very rapidly upon $Mn-CO_{ax}$ bond lengthening and crosses the $d_{\pi^*} \rightarrow \sigma^*$ states already shortly after 2.0 Å. Ultimately, in $Mn_2(CO)_9$, the LF excitation is even much lower than the original $d_{\pi^*} \rightarrow \sigma^*$ excitation in $Mn_2(CO)_{10}$, releasing sufficient energy to break the Mn−CO bond. The dissociation of axial CO along the $^{1,3}E$ PECs proceeds barrierless due to the crossing to LF character taking place close to the equilibrium $Mn-CO_{ax}$ distance.

Dissociation of an equatorial CO may also occur but less readily. Due to the symmetry lowering the E states now split into A′ and A″ states. Again, the $\sigma \rightarrow \sigma^*$ excited states (a^3A', b^1A') are not dissociative with respect to the $Mn-CO_{eq}$ bond, but the b^3A' component of the $d_{\pi^*} \rightarrow \sigma^*$ $^3E_1$ state is dissociative; although its PEC is different from the corresponding ^3E for axial CO, it is very flat and has to pass a low barrier. In the same way as for axial CO, the $d_{\pi^*} \rightarrow \sigma^*$ $^3E_1-b^3A'$ state evolves into a LF type excited state, this time to a localized $d^1_{x^2-y^2}$ orbital. We note that the equatorial $d^1_{x^2-y^2}$ is in $Mn_2(CO)_{10}$ considerably higher than the axial $d^1_{z^2}$ (see ref 16); it comes down somewhat more slowly upon Mn−CO bond lengthening so that a barrier can develop in the $d_{\pi^*} \rightarrow \sigma^*$ $^3E_1-b^3A'$ PEC. Asymptotically the LF excited state to the equatorial $d^1_{x^2-y^2}$ is somewhat higher than that to the axial $d^1_{z^2}$, and the $^3E_1-b^3A'$ PEC is less clearly dissociative than the $^{1,3}E_1-^{1,3}E$ PECs for axial dissociation. This may be summarized in the picture that the pushing up effect of the CO lone pairs (5σ) on the axial $d^1_{z^2}$ is already diminished in $Mn_2(CO)_{10}$, by the replacement of one CO in the octahedral environment by the $Mn(CO)_5$ unit, $d^1_{z^2}$ therefore being lower than $d^1_{x^2-y^2}$ all along the $Mn-CO_{ax}$ and $Mn-CO_{eq}$ coordinate, respectively. Hence a downward shift of the $d^1_{z^2}$ LF excited state compared to the $d^1_{x^2-y^2}$ LF excited state, leading to the above noted consequence of more readily dissociating axial CO.

It is interesting to note that the phenomenon of CO dissociation upon excitation into the low-energy bands of $Mn_2(CO)_{10}$ has led Meyer and Caspar[66] to examine the possibility that these low-energy excitations include LF type excitation to $d^1_{x^2-y^2}$. We have ruled out this possibility on the basis of our calculated excitation energies (note the high $\sigma \rightarrow d_\delta$ and $d_\pi \rightarrow d_\delta$ excitation energies in Figures 8 and 10), but the suggestion in a sense foreshadows the precipitous lowering of the LF excited states with Mn−CO bond lengthening that we find to play such a crucial role in the dissociation.

Our findings account for the occurrence of two primary photoprocesses for $Mn_2(CO)_{10}$ in the range 337−355 nm, with the molecule undergoing either the metal−metal bond homolysis or the loss of a carbonyl ligand, most probably the axial one. The intersection of the $\sigma \rightarrow \sigma^*$ $^1B_2$ and $8e_3 \rightarrow 10b_2$ $^3E_1$ surfaces enables both photoprocesses to occur independently of the excitation wavelength in this range, which nicely agrees with the experimental findings.

Irradiation of $Mn_2(CO)_{10}$ at $\lambda \leq 266$ nm may bring the molecule directly or indirectly into excited states that are strongly $Mn-CO_{ax}$ or $Mn-CO_{eq}$ antibonding, i.e., which lower their energy steeply upon Mn−CO bond stretching. This may start the Mn−CO dissociation process, during which the system may electronically relax to one of the dissociative low-energy excited states we have just discussed. No photoactive state for Mn−Mn bond homolysis is found in this high-energy region. Thus the only photochemical process that we predict upon excitation of $Mn_2(CO)_{10}$ in the high-energy region is the loss of a carbonyl ligand, which is in agreement with gas-phase photoexperiments[15] in that excitation of $Mn_2(CO)_{10}$ at 248 and 193 nm leads to ligand loss with no evidence of metal−metal homolysis. The interpretation of condensed-phase experiments that establish the occurrence, although with a very low quantum yield, of the metal−metal homolysis, when exciting $Mn_2(CO)_{10}$ at 266 nm,[14] would involve the assumption of low-probability crossing, due to the perturbative effect of the solvent, to the Mn−Mn dissociative states at low energy.

Acknowledgment. We gratefully acknowledge a grant of computer time by the foundation Nationale Computer Faciliteiten (NCF) of the Netherlands Foundation for Scientific Research (NWO). This work was supported by the HCM network "Quantum Chemistry of Transition Metal Complexes", No. ERBCHRXCT 930156.

IC950518H

(66) Meyer, T. J.; Caspar, J. V. *Chem. Rev.* **1985**, *85*, 187.